Northumbria Research Link

Self-consistent fractal geometry in polyampholyte hydrogels undergoing exchange and correlation charge-density

Ziyu Xing[1], Haibao Lu[1,*] and Yong-Qing Fu[2,*]

[1]National Key Laboratory of Science and Technology on Advanced Composites in Special Environments, Harbin Institute of Technology, Harbin 150080, China

[2]Faculty of Engineering and Environment, University of Northumbria, Newcastle upon Tyne, NE1 8ST, UK

[*]Corresponding author, E-mail: luhb@hit.edu.cn and richard.fu@northumbria.ac.uk

Abstract: Polyampholyte (PA) hydrogels are incorporated of many internally charged polymer chains, which play an important role to influence the fractal networks and dynamic elasticity of the PA hydrogels owing to their different exchange and correlation charge-densities. Many properties of the PA hydrogels, such as mechanical strength and deformation, are significantly dependent on their fractal networks. However, working principles of chemo-mechanical coupling between the fractal networks and the elasticity of PA hydrogels have not been fully understood. In this study, a self-consistent fractal geometry model integrated with a complex function is proposed to understand the constitutive relationship between dynamic networks and tailorable mechanics in the PA hydrogels. The newly developed model is uniquely incorporated with the mechanochemistry, and describes the chemical polarization reactions of charged networks and their mechanical behaviors using complex fractal functions. Based on the rubber elasticity theory, constitutive stress-strain relationships of fractal networks have been described using their elastic, conformational, repulsive

and polarization free-energy functions. Finally, effectiveness of the proposed model has been verified using both finite element analysis (FEA) and experimental results of the PA hydrogels reported in literature.

Keywords: polyampholyte; self-consistent; charge-density; fractal geometry

1. Introduction

As one of the most popular soft matters, hydrogels are composed of three-dimensional polymer networks containing a large amount of water, with capabilities of large deformation and good biocompatibility [1-5]. They have various functional properties, including self-assembly [6], liquid crystal behavior [7], non-swellablility [8], self-healing [9] and electrical conductivity [10]. Therefore, they have been explored for wide-range applications, including artificial muscles [4], medical scaffold [9], battery [11], wound dressing [12], soft robotics [13] and soft actuators [14].

However, the bottleneck for their successful applications is their poor mechanical properties. To obtain tough and strong hydrogels, many approaches have been adopted by means of grafting [8,15], sacrificial bonding [16-18] and phase-separation [19]. Experimental studies reveal that polyampholyte (PA) hydrogel present a Young's modulus value as high as 10 times in comparison with those of the standard ones [18,20-22] (whose the Young's moduli are normally about 10 kPa [20-22]). The PA hydrogels with ionic bonds also show reversibly self-repairing properties during their mechanical cycling [23-26].

Many studies have reported on the toughening mechanisms, and a series of phenomenological and physical models have been formulated to describe the effects of ionic bonds on the mechanical properties of PA hydrogels [24-32]. However, mechanochemistry relationships between their ionic bonds and mechanical properties have not been well understood, mainly due to their scaling effects [33-35]. In the previous studies [36,37], mechanochemistry of polyelectrolyte (PE) and PA hydrogels has been investigated to explore their working principles of multi-field coupling effects, thus providing a fundamental approach to understand their thermodynamics of mechanochemistry. For example, simulation studies have been done for the deformation behavior of PE hydrogels in the presence of mechanical contraction after being bound with electrostatically attractive viral particles [36]. Another study was done to investigate the critical-adsorption conditions of PA chains onto spherical particles [37]. Currently, it is critically needed to explore their constitutive relationship between mechanical property and network structure, which is determined by the exchange and correlation charge-density. The thermodynamic elasticity of polymer network plays an essential role to determine mechanical behaviors of these PA hydrogels. However, currently few studies have been carried out to identify the toughening mechanisms of mechanochemistry, which is mainly originated from a complex coupling and scaling effects between molecular chemistry in network and macroscopical mechanics of these PA hydrogels [38-40].

In this study, a self-consistent fractal geometry model is proposed to understand the constitutive relationship between network structure and mechanical elasticity in the

PA hydrogel undergoing exchange and correlation charge-density. Initially, a free-energy equation has been formulated to identify the thermodynamics of polymer networks undergoing exchange and correlation charge-density in PA hydrogel [33-35,38]. A fractal geometry model is then developed to describe the constitutive relationship between charge-density and geometrical shape of the network structures by using the fractal function and rubber elasticity theory [39-41]. Finally, effectiveness of the proposed model is verified using both finite element analysis (FEA) and experimental results of PA hydrogels reported in the literature.

2. Theoretical framework

Charge-density in the PA hydrogels has a decisive influence on their mechanical properties. Electric field ($E(z)$) is determined by the charge diffusion distance (z) and Gouy-Chapman length (L_{GC}) [33-35], which can be written as following,

$$E(z) = \frac{4\pi e S_c}{\varepsilon_d} \frac{L_{GC}}{z + L_{GC}} \tag{1a}$$

$$L_{GC} = \frac{\varepsilon_d k_B T}{2\pi e^2 S_c} \tag{1b}$$

where S_c is surface charge-density, ε_d is the dielectric constant, $e=1.6\times10^{-19}$ C is the charge quantity, $k_B=1.38\times10^{-23}$ J/K is the Boltzmann constant and T is the temperature. The conformational free energy ($F_c(z)$) [39] and polarization free energy ($F_p(z)$) [33-35] of the PA chains in the electric field can be described using the following equations,

$$F_c(z) = k_B T \frac{h^2(z)}{Nb^2} \tag{2}$$

$$F_p(z) = -e\sqrt{fN}h(z)E(z) \tag{3}$$

where $h(z)$ is the end-to-end distance of chain, N is the number of segments, b is the length of a segment and f is the concentration of charge.

Here, the end-to-end distance ($h(z)$) of PA chain can be expressed as [33-35],

$$h(z) = \frac{Nb^2 \sqrt{fN}}{z + L_{GC}} \tag{4}$$

Substituting equation (4) into (3), the polarization free energy (F_p) is obtained as,

$$F_p(z) = -e\sqrt{fN}h(z)E(z) = -k_BT(\frac{f^{0.5}Nb}{z + L_{GC}})^2 \tag{5}$$

Owing to the thermodynamic equilibrium of three-body contact and polarization effect [33], there is a repulsive free energy ($F_r(z)$), which is determined by the chain density ($\rho(z)$),

$$F_r(z) = k_BTNb^6\rho^2(z) = k_BT(\frac{f^{0.5}Nb}{z + L_{GC}})^2 \tag{6}$$

$$\rho(z) = \frac{1}{b^2}\frac{\sqrt{fN}}{z + L_{GC}} \tag{7}$$

Substituting equation (5) into (6), the repulsive free energy ($F_r(z)$) has a constitutive relationship with polarization free energy ($F_p(z)$), which is $F_r(z)=-F_p(z)$ [33-35].

As it is known, the thermodynamics of polymer networks is determined by their geometrical shapes [33-35,38], which are originated from the exchange and correlation charge-density with the external solvent system. Therefore, it is necessary to describe the geometrical shapes of network structures, whose free energies are determined by their charge-densities. Here, a complex fractal function ($Z=|(X+iY)^2+c|$) is employed to characterize the geometrical shapes of network structures undergoing

exchange charge-density, as shown in Figure 1. X and Y represent the coordinates for

the complex plane. $i = \sqrt{-1}$ and c are the given constants for the geometrical fractals

of network structures.
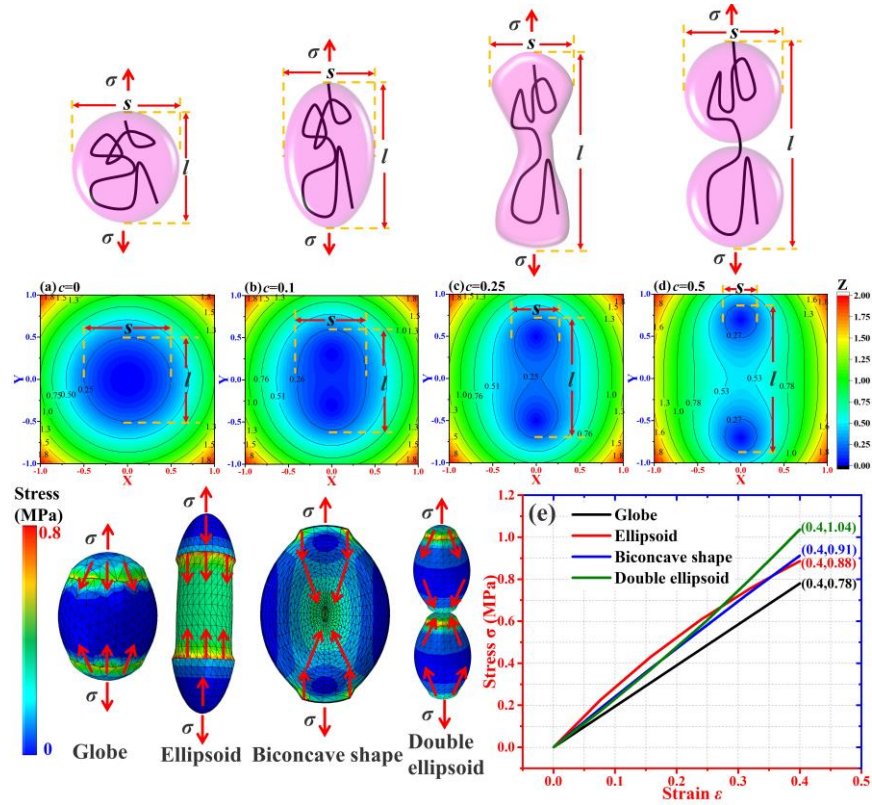
Figure 1. FEA simulations of network structures and stress-strain curves in the PA hydrogel

undergoing globe, ellipsoid, biconcave and double ellipsoid fractals. (a) Geometrical shape of

globe fractal with c=0 in the complex fractal function. (b) Geometrical shape of ellipsoid fractal

with c=0.1 in the complex fractal function. (c) Geometrical shape of biconcave fractal with c=0.25

in the complex fractal function. (d) Geometrical shape of double ellipsoid fractal with c=0.5 in the

complex fractal function. (e) The stress-strain curves of network structures with globe, ellipsoid,

biconcave and double ellipsoid fractals in PA hydrogels.

Finite-element analysis (FEA) simulations are performed to analyze the globe,

ellipsoid, biconcave and double ellipsoid fractals of the networks, which are shown in

Figures 1(a), 1(b), 1(c) and 1(d), respectively. In the simulations, the corresponding complex fractal functions are selected as $c=0$, $c=0.1$, $c=0.25$ and $c=0.5$, respectively. The Poisson's ratio is chosen as 0.45 [39] and the modulus is chosen as 1 MPa for the PA hydrogel. In this paper, a unified mathematical equation of complex fractal function $Z=|(X+iY)^2+c|$ is employed to describe the fractal geometry of polymer networks, of which the fractal shape is determined by the exchange and correlation charge-density. In this complex fractal function, c is a given real constant, i is the imaginary number, and the parameters X and Y are used to determine the two-dimensional (2D) fractal geometry of polymer networks. Furthermore, FEA simulation has been applied to characterize the fractal geometry and mechanical elasticity of polymer networks. As can be seen from the FEA model shown in Figure 1(e), the geometric shape of polymer network can be determined using the FEA simulation. With the increase of c from 0, 0.1, 0.25 to 0.5, four types of geometric shapes can be obtained, i.e., globe, ellipsoidal, biconcave and double ellipsoidal ones, with the obtained results shown in Figures 1(a), 1(b), 1(c) and 1(d), respectively.

Based on the experimental results [18-23] and theory of conformational entropy [33-37], the polymer network undergoes an ellipsoidal shape deformation, resulted from the repulsive free energy of charge-density. Whereas the uncharged polymer network always presents a globe shape (where $c=0$ in the complex fractal function), owing to its elastic and mixing free-energy functions. Therefore, the globe and ellipsoid shapes are employed to describe the polymer networks in the PA hydrogels, of which the exchange and correlation charge-density are tailorable and designable.

On the other hand, a fractal function, which is self-consistent, has been employed to characterize the polymer network undergoing a geometrical shape from the ellipsoid (c=0.1), biconcave (c=0.25) to double ellipsoid (c=0.5) fractals in responses to the exchange and correlation charge-density.

An 8-node hexahedron element, C3D8R, was used to perform the FEA simulation for the three-dimensional structures. About 12000 elements were used to model the whole unit of polymer networks [42,43]. Fractal geometric equations in real space used in FEA simulation have been presented in equations (S1), (S2) and (S3) in the Supporting Material. The possible limitation using the element of C3D8R is that the FEA simulation results generated from 1-point integration often fail to obtain those of each single unit. The color-bars of the FEA results are used to characterize the stress distribution of the polymer networks in responses to the exchange and changes of charge-density. Whereas, the contour plot, which is determined by the complex fractal function of $Z=|(X+i\text{Y})^2+c|$, is used to present the divergence in the speed of the fractal geometry for the polymer network. Figure 1(e) shows the simulated mechanical stresses as a function of strain for the PA hydrogels. The geometrical shapes of network structures are selected to have globe, ellipsoid, biconcave and double ellipsoid fractals. FEA simulation results show that the tensile stresses are increased from 0.78 MPa, 0.88 MPa, 0.91 MPa to 1.04 MPa for the networks undergoing globe, ellipsoid, biconcave and double ellipsoid fractals, respectively, at the same strain of 40%. These simulation results prove that the geometrical shape of network structure significantly influences the mechanical property of the PA hydrogel. Owing to the

exchange and correlation charge-densities, the geometrical fractal of network structure then enables different constitutive stress-strain relationships and a variety of mechanical properties, which have been verified by the FEA simulation results. Self-consistency is one of the inherits in fractal theory, of which the complex fractal function is employed to characterize the geometrical shapes of polymer networks. With the exchange and correlation of charge-density, the geometrical shape of network structures is varied owing to the repulsive free energy.

Considering the polymer chains in the PA hydrogels with ellipsoid shapes, the long axis of the chain can be denoted as l and the short axis can be denoted as s, therefore, the modulus (E_r) of the PA hydrogel is expressed as [44],

$$\frac{1}{E_r} = \frac{4(1-\phi)}{G_c \phi^2 k_{l/s}^2} + \frac{1}{\phi E_w} \tag{8}$$

where $k_{l/s}=l/s$, which has been employed to characterize the geometric shapes of polymer networks. Here l is the major axis and s is the minor axis of ellipsoid polymer network. ϕ is the volume fraction of polymer chain, G_c is the shear modulus ratio and E_w is the modulus ratio of water to gel in PA hydrogel. Based on the given constant of $k_{l/s}=l/s$, the geometric characteristics of polymer networks are determined, and the complex fractal function can be obtained by the constitutive relationship between $k_{l/s}$ and c. When c is determined, the values of X and Y can be obtained according to the contour plot of Z function. The shape of polymer network can be determined by $k_{l/s}=l/s$. All the obtained data can be further applied to FEA simulations.

According to the continuum mechanics [27], the end-to-end distance ($h(z)$) of polymer chain can be described by the elongation ratio as,

$$h(z) = h(z_0)\sqrt{\frac{I_1}{3}} \tag{9a}$$

$$I_1 = \lambda_1^2 + \lambda_2^2 + \lambda_3^2 \tag{9b}$$

where $h(z_0)$ is the initial end-to-end distance, I_1 is the strain invariant, λ_1, λ_2 and λ_3 represent the elongation ratios along three directions, respectively. In combination of equations (2), (6), (8) and (9), the free energy (F_z) can be expressed as,

$$F_z = F_r + F_c = \frac{Nk_BT}{\dfrac{4(1-\phi)}{G_c\phi^2 k_{l/s}^2} + \dfrac{1}{\phi E_w}}\frac{Nfb^2}{(z_0+L_{GC})^2}\sqrt{\frac{I_1}{3}} + Nk_BT\frac{Nfb^2}{(z_0+L_{GC})^2}\frac{I_1}{3} \tag{10}$$

By integrating the parameter z with the external force, the free energy (F_{zm}) of molecular network undergoing the deformation is,

$$\frac{F_{zm}}{Nk_BT} = \frac{\int_0^\infty F_z dz_0}{Nk_BT\cdot\sqrt{Nb}} = \frac{f\sqrt{Nb}/L_{GC}}{\dfrac{4(1-\phi)}{G_c\phi^2 k_{l/s}^2} + \dfrac{1}{\phi E_w}}\sqrt{\frac{I_1}{3}} + \frac{f\sqrt{Nb}}{L_{GC}}\frac{I_1}{3} \tag{11}$$

Meanwhile, according to the rubber elasticity theory [40,41], elastic free energy (F_{el}) is obtained,

$$F_{el} = 3N_{el}k_BT[\frac{I_1}{6} + \beta^{-1}(1-\frac{\beta I_1}{3})^{-1}] \tag{12}$$

where N_{el} is the number of chains and β is a material constant. In combination of equations (11) and (12), the total free energy (F_{PA}) of PA hydrogel is obtained,

$$F_{PA} = F_{zm} + F_{el} =$$
$$Nk_BT[\frac{f\sqrt{Nb}/L_{GC}}{\dfrac{4(1-\phi)}{G_p\phi^2 k_{l/s}^2} + \dfrac{1}{\phi E_w}}\sqrt{\frac{I_1}{3}} + \frac{f\sqrt{Nb}}{L_{GC}}\frac{I_1}{3}] + 3N_{el}k_BT[\frac{I_1}{6} + \beta^{-1}(1-\frac{\beta I_1}{3})^{-1}] \tag{13}$$

According to the assumption of volume invariance for the isotropic material, i.e., $\lambda_1\lambda_2\lambda_3=1$, the constitutive relationship of stress (σ_u) as a function of elongation ratio (λ) for the PA hydrogel undergoing the uniaxial tensile stretching can be finally achieved,

$$\frac{\sigma_u}{N_{el}k_BT} = \frac{\partial F_{PA}/N_{el}k_BT}{\partial \lambda} = (\lambda - \frac{1}{\lambda^2})\left[1 + 2(1-\beta\frac{\lambda^2 + 2/\lambda}{3})^{-2}\right]$$
$$+ \frac{fN^{3/2}b}{N_{el}L_{GC}}(\lambda - \frac{1}{\lambda^2})[\frac{2}{3} + \frac{E_r}{\sqrt{3}}(\lambda^2 + \frac{2}{\lambda})^{-0.5}] \tag{14}$$

To verify the proposed model of equation (14), it has been used to analyze the mechanical behavior of PA hydrogels. The obtained results are plotted in Figure 2, in which the constitutive stress-strain relationships are varied. All the parameters used in the equation (14) for calculations are $N_{el}k_BT$=0.1MPa, β=0.003, $fN^{3/2}b/N_{el}L_{GC}$=3, ϕ=0.5, E_w=1 and G_p=2. Results showed that the stress of PA hydrogel is increased from 2.88 MPa, 3.14 MPa, 3.30 MPa, 3.39 MPa to 3.45 MPa at the same elongation ratio of λ=7, with an increase of $k_{l/s}$ from 1 to 5. The analytical results using the equation (14) reveal that the stress of PA hydrogel has been enhanced with an increase in the $k_{l/s}$, which can be used to describe the effects of geometrical shape and fractal of the polymer networks. The value of $k_{l/s}$ gradually increases with the development of fractal geometry from globe, ellipsoid, biconcave to double ellipsoid. The complex fractal geometry can be described by $k_{l/s}$, and the evolution of fractal geometry under stress is represented by introducing geometric parameter $k_{l/s}$ into the model. As explained above, a higher value of $k_{l/s}$ is linked with the increased polarization of polymer chains, which results in the transformations from globe, ellipsoid, biconcave to double ellipsoid fractal, and the mechanical stress is therefore increased.
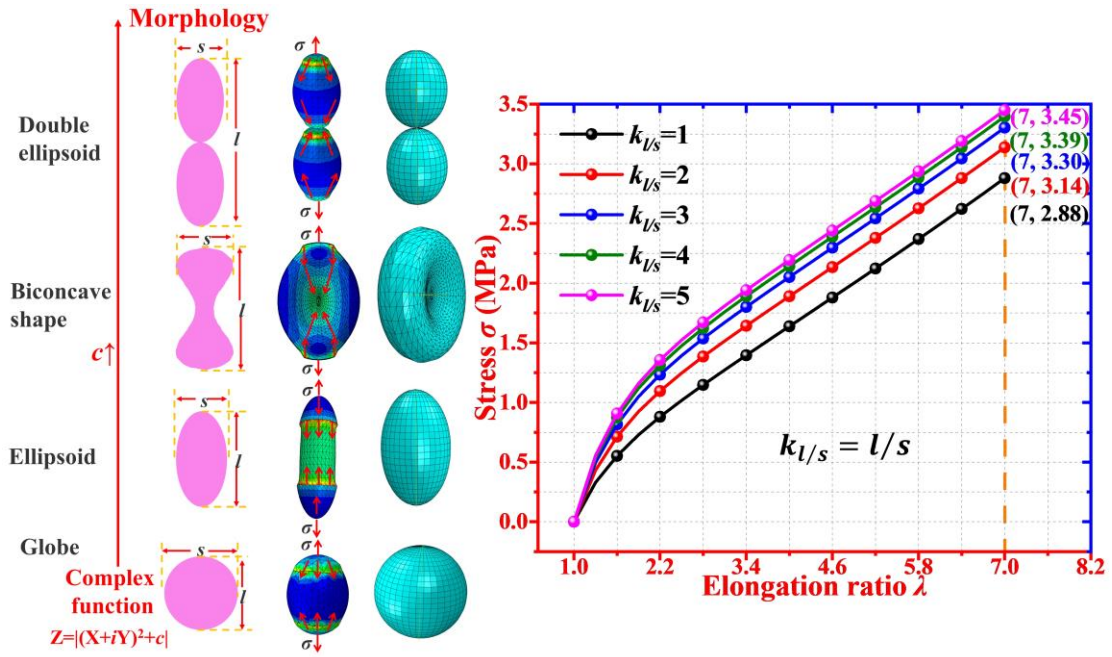
Figure 2. Analytical results of equation (14) for the PA hydrogels with various length-diameter ratio of l/s of $k_{l/s}=1$, $k_{l/s}=2$, $k_{l/s}=3$, $k_{l/s}=4$ and $k_{l/s}=5$, where the network with geometrical shapes of globe, ellipsoid, biconcave and double ellipsoid fractals.

To further investigate effect of exchange and correlation charge-density on the mechanical behaviour of PA hydrogel, two parameters, i.e., concentration of charged monomers (f) and Gouy-Chapman length (L_{GC}) have been studied based on equation (14). Parameters used in equation (14) for the calculations are $N_{el}k_BT$=0.1 MPa, β=0.024, $N^{3/2}b/N_{el}L_{GC}$=30, $fN^{3/2}b/N_{el}$=30 nm and E_r=1. Figure 3(a) shows the analytical results of the stress-strain curves for the PA hydrogels with various concentrations of charged monomers (f) from 0.10, 0.15, 0.20, 0.25 to 0.30, calculated using equation (14). Results show that the stress values are increased from 6.07 MPa, 6.86 MPa, 7.64 MPa, 8.42 MPa to 9.21 MPa with the increase of concentrations of charged monomers in the PA hydrogels, at the same elongation ratio of λ=7. Results also show that with an increase in the concentration of charged monomers (f), the free

energy (F_{zm}) of PA hydrogel is significantly increased owing to the increased polarization and repulsive free energies, as predicted from equation (11).

Meanwhile, effect of Gouy-Chapman length (L_{GC}) on the mechanical behavior of PA hydrogel is also investigated using equation (14), and the obtained results are presented in Figure 3(b). Results reveal that the stress is gradually decreased from 8.42 MPa, 6.74 MPa, 6.07 MPa, 5.71 MPa to 5.48 MPa with an increase in the Gouy-Chapman length (L_{GC}) from 4 nm, 7 nm, 10 nm, 13 nm to 16 nm. As explained above, with an increase in the Gouy-Chapman length (L_{GC}), the free energy (F_{zm}) of PA hydrogel is decreased, mainly due to the decreases in polarization and repulsive free energies.

The relationship between fractal geometry and electrical parameters can be well predicted using the model of equation (14). The effects of concentration of charged monomers (f) and Gouy-Chapman length (L_{GC}) on the end-to-end distance ($h(z)$) of the fractal network of PA hydrogel is shown in Equation (4) [33-35]. With the increase of concentration of charged monomers (f), end-to-end distance ($h(z)$) is increased, which indicates that more double ellipsoidal fractals are produced under the action of electric field, leading to the enhanced mechanical properties due to electrostatic repulsion. However, the increase of Gouy-Chapman length (L_{GC}, which represents dielectric properties) leads to the decrease of the end-to-end distance ($h(z)$), and the fractal tends to become globe shape. The proposed model can well describe the effects of exchange and correlation charge on end-to-end distance ($h(z)$) according to the connection of fractal geometry to charge density.
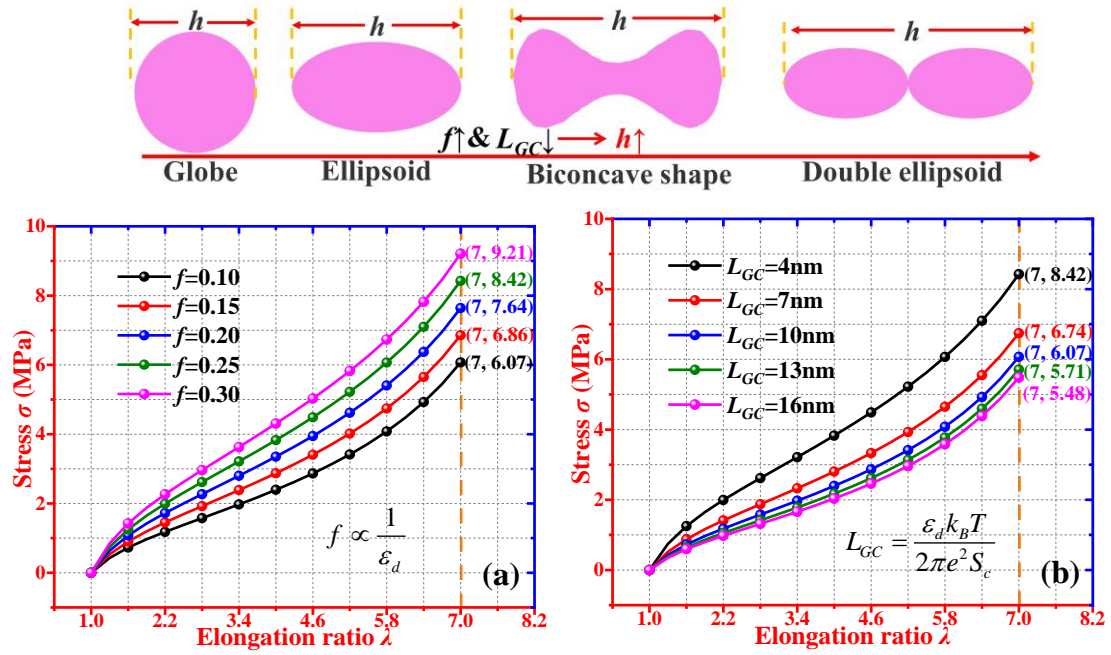
Figure 3. (a) Analytical results of stress as a function of elongation ratio for the PA hydrogel with various concentrations of charged monomers (f). (b) Analytical results of stress as a function of elongation ratio for the PA hydrogel with various Gouy-Chapman lengths (L_{GC}).

3. Experimental verification

3.1 Materials

Two groups of experimental data of PA hydrogels undergoing exchange and correlation charge-density (reported in Ref. [18,45]) have been collected to verify the analytical results generated from the proposed model, namely; (1) poly(NaSS-co-MPTC) PA hydrogel [18], where NaSS represents sodium p-styrenesulfonate and MPTC represents 3-(methacryloylamino) propyltrimethylammonium chloride. As reported in Ref. [18], the exchange and correlation charge-density of the poly(NaSS-co-MPTC) PA hydrogels are originated from the ionic balance in solution; (2) poly(NaSS-co-DMAEA-Q) PA hydrogel [45], where NaSS represents sodium p-styrenesulfonate and DMAEA-Q represents

dimethylaminoethylacrylate quaternized ammonium. As reported in Ref. [45], the exchange and correlation charge-density of the poly(NaSS-co-DMAEA-Q) PA hydrogels is originated from the concentrations of multivalent cations in solution.

Here, $N_{el}k_BT$ is the modulus introduced by rubber elasticity theory [39-41], N_{el} is the number of chains undergoing ion crosslink in the PA hydrogel, k_B=1.38×10^{-23} J/K is the Boltzmann constant, T≈298.15 K is the ambient temperature, β is a material constant which indicates the limit of chain at a fully extended state [40,41], $\dfrac{fN^{3/2}b}{N_{el}L_{GC}}$ is the coefficient of PA hydrogel undergoing exchange and correlation charge-density , N is the number of segments, b≈1 nm is the length of a segment [33-35] and f is the concentration of charge, L_{GC}≈10 nm is Gouy-Chapman length [33-35], $k_{l/s}$ is length-diameter ratio of l/s [44], ϕ=0.2 is the volume fraction of polymer chain [44], G_c=100 is the shear modulus ratio and E_w=400 is the modulus ratio of gel to water in PA hydrogel [44]. As discussed in Figures 2 and 3, changes of fractal structure can be explained in detail using the equations (4) and (8), which determine the end-to-end distance and long-short axis ratio, as well as the transformation of fractal networks.

3.2 Effect of univalent cation on fractal geometry in PA hydrogel

To verify the proposed model based of equation (14), the experimental data [18] for the poly(NaSS-co-MPTC) PA hydrogel reported in Ref. [18] have been employed to compare with the analytical results based on the proposed model. Figure 4(a) plots the theoretically obtained relationships between tensile stress and elongation ratio of the poly(NaSS-co-MPTC) PA hydrogels with various concentrations of NaCl, i.e., 0 mol/L, 0.06 mol/L, 0.15 mol/L, 0.3 mol/L and 0.5 mol/L. All the parameters used in

the calculation of equation (14) are listed in Table 1.

Table 1. Values of parameters used in equation (14) for poly(NaSS-co-MPTC) PA hydrogel with various concentrations of NaCl.

NaCl (mol/L)	$N_{el}k_BT$ (kPa)	β	$\dfrac{fN^{3/2}b}{N_{el}L_{GC}}$	$k_{l/s}$
0	46.5			2.40
0.06	29.4			2.10
0.15	16.9	0.007	1	2.09
0.3	8.9			2.05
0.5	2.7			2.00

Both the analytical and experimental results show that the tensile stress of poly(NaSS-co-MPTC) PA hydrogel is decreased from 2.52 MPa, 1.66 MPa, 0.94 MPa, 0.48 MPa to 0.14 MPa with an increase in the concentration of NaCl from 0 mol/L, 0.06 mol/L, 0.15 mol/L, 0.3 mol/L to 0.5 mol/L, at the same elongation ratio of λ=10. Results reveal that the NaCl plays an essential role to influence the charge-density, resulting in the dramatic decrease of thermodynamic free energy for the polymer networks and changes of the geometrical shapes from ellipsoid to globe owing to the neutralization reaction between NaCl and PA hydrogel [18]. Therefore, the tensile stress of poly(NaSS-co-MPTC) PA hydrogel is decreased with an increase in the concentration of NaCl, mainly due to the decrease in the charge-density. The simulation results fit well with the experimental data with errors limited to $|\Delta\sigma|$<0.20 MPa. The divergences between the analytical and experimental results of the poly(NaSS-co-MPTC) PA hydrogels were calculated using the correlation index (R^2), and the obtained results shown in Figure 4(b) are 98.75%, 99.59%, 99.46%, 98.02% and 98.51% for concentrations of NaCl of 0 mol/L, 0.06 mol/L, 0.15 mol/L, 0.3 mol/L

and 0.5 mol/L, respectively. The working principles of different concentrations of NaCl in the poly(NaSS-co-MPTC) PA hydrogel are illustrated in Figure 4(c). With an increase in the concentration of NaCl, the charge-density is gradually decreased owing to the neutralization reaction between NaCl and poly(NaSS-co-MPTC) PA hydrogel, thus resulting in the transformation of geometrical shape of network structure from ellipsoid to globe. Therefore, the tensile stress of the hydrogel is decreased with an increase in the concentration of NaCl, resulted from the transformation of geometrical shapes of the network structures.
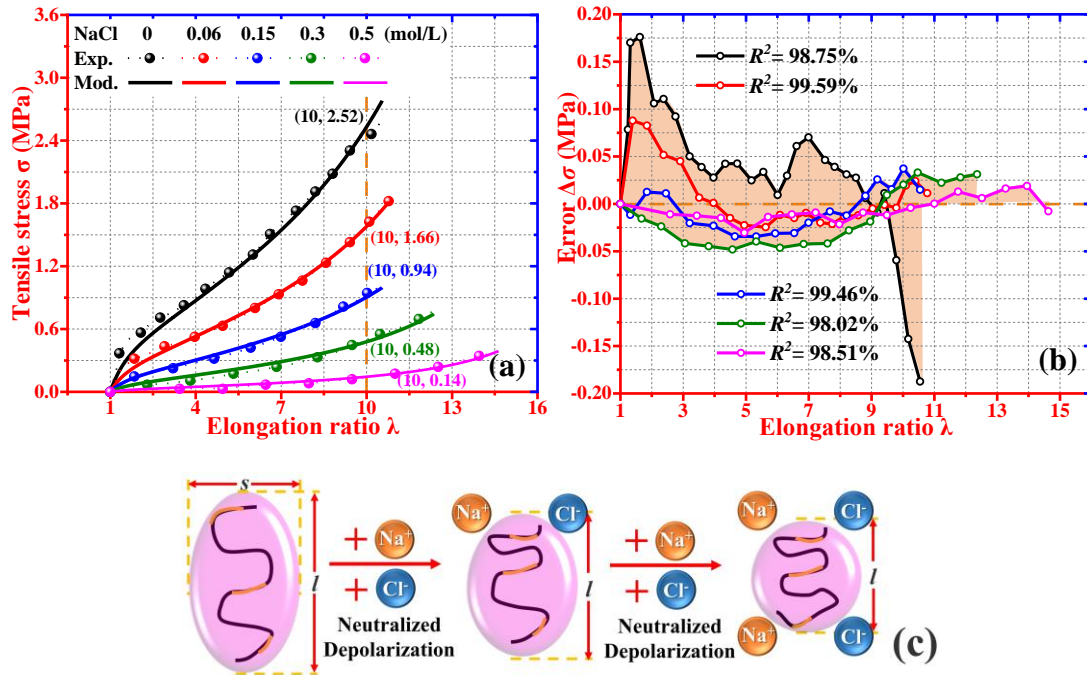
Figure 4. Effect of NaCl concentration on the constitutive tensile stress-elongation ratio relationship of poly(NaSS-co-MPTC) PA hydrogel with the NaCl concentrations of 0 mol/L, 0.06 mol/L, 0.15 mol/L, 0.3 mol/L and 0.5 mol/L. (a) The stress-elongation ratio curves. (b) Divergences of analytical and experimental results [18] of tensile stress. (c) Schematic illustrations of geometrical fractals of network structures in the poly(NaSS-co-MPTC) PA hydrogels with different concentrations of NaCl.

3.3 Effect of multivalent cations on fractal geometry in PA hydrogel

Furthermore, effect of multivalent cations on fractal geometry of polymer network has also been investigated for the PA hydrogel [45]. It is expected that the multivalent cation plays an inherently different role to influence the exchange and correlation charge-density in comparison with that of univalent cation, resulting into distinct differences in fractal geometry and mechanical elasticity of polymer network.

Analytical results of tensile stress as a function of elongation ratio obtained using equation (14) are plotted in Figure 5(a), which also includes the experimental data of poly(NaSS-co-DMAEA-Q) PA hydrogels with various concentrations of $FeCl_3$ reported in Ref. [45]. All the parameters used in the simulations using the equation (14) are listed in Table 2. Both the analytical and experimental results show that the tensile stress of poly(NaSS-co-DMAEA-Q) PA hydrogel is significantly increased from 0.15 MPa, 0.47 MPa, 0.74 MPa, 1.26 MPa to 1.69 MPa, with an increase in the concentration of $FeCl_3$ from 0 mol/L, 0.3 mol/L, 0.5 mol/L, 0.7 mol/L to 2 mol/L, at the same elongation ratio of λ=6.1. Based on the experimental observations, the Fe^{3+} and Cl^- ions react with polymer chains and thus increase the charge-density of PA hydrogels [45]. This helps the increase of the polarization free energy of polymer chains, thus effectively increasing the tensile stress. In this case, the $FeCl_3$ is used to enhance the charge-density in the poly(NaSS-co-DMAEA-Q) PA hydrogel, whereas NaCl is used to decrease the charge-density in poly(NaSS-co-MPTC) PA hydrogels due to the neutralization reactions between NaCl and PA hydrogel [18].

For comparisons of these results, the divergences between the analytical and

experimental results of the poly(NaSS-co-DMAEA-Q) PA hydrogels are calculated

using the correlation index (R^2), which are 94.75%, 96.32%, 98.03%, 96.87% and

98.90% for concentrations of $FeCl_3$ from 0 mol/L, 0.3 mol/L, 0.5 mol/L, 0.7 mol/L

and 2 mol/L, respectively, as shown in Figure 5(b). These results indicate a good

agreement between analytical and experimental results.

Table 2. Values of parameters used in equation (14) for poly(NaSS-co-DMAEA-Q) PA hydrogel

with various concentrations of $FeCl_3$.

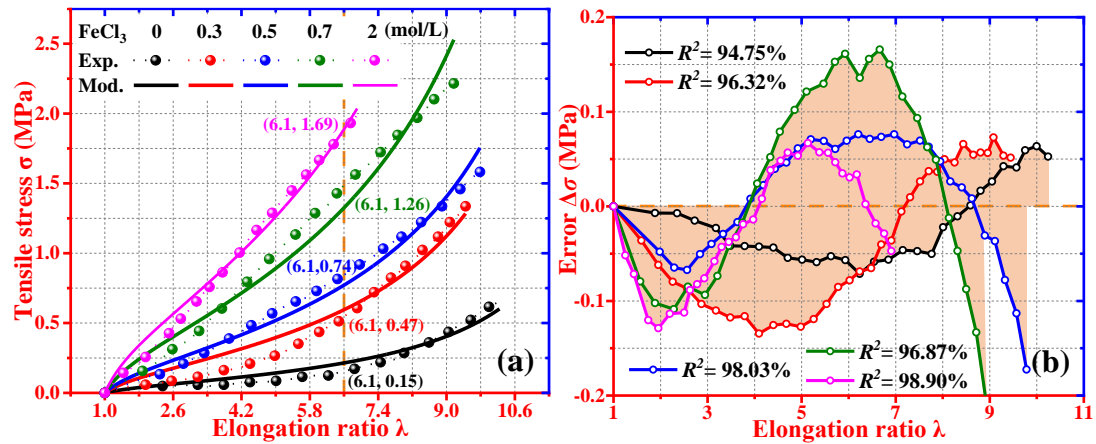| $FeCl_3$ (mol/L)	$N_{el}k_BT$ (kPa)	β	$\dfrac{fN^{3/2}b}{N_{el}L_{GC}}$	$k_{l/s}$
0	8.0			1.10
0.3	22.3			1.15
0.5	29.5	0.012	0.1	1.20
0.7	50.7			1.25
2	71.3			1.30

Figure 5. Effect of $FeCl_3$ concentration on the constitutive tensile stress-elongation ratio

relationship of poly(NaSS-co-DMAEA-Q) PA hydrogel, where the concentrations of $FeCl_3$ are 0

mol/L, 0.3 mol/L, 0.5 mol/L, 0.7 mol/L and 2 mol/L. (a) The tensile stress-elongation ratio curves.

(b) Divergences of analytical and experimental results [45] of tensile stress.

For the applications of PA hydrogels, it is also critical to understand their tearing

deformation behaviors [45]. During the tearing loading, the volume of PA hydrogel is kept a constant, i.e., $\lambda_1\lambda_2\lambda_3=1$, $\lambda_1=\lambda$, $\lambda_2=\lambda^{-1}$ and $\lambda_3=1$. This will result in the first strain invariance, i.e., $I_1=\lambda^2+1/\lambda^2+1$, which is illustrated in Figure 6(a). Based on the equation (13), the constitutive relationship of tearing stress (σ_s) as a function of elongation ratio (λ) can be obtained,

$$\frac{\sigma_s}{N_{el}k_BT} = \frac{\partial F_{PA}/N_{el}k_BT}{\partial(\lambda-1/\lambda)} = (\lambda-\frac{1}{\lambda})\left[1+2(1-\beta\frac{1+\lambda^2+1/\lambda^2}{3})^{-2}\right] \\ +\frac{fN^{3/2}b}{N_{el}L_{GC}}(\lambda-\frac{1}{\lambda})[\frac{2}{3}+\frac{E_r}{\sqrt{3}}(1+\lambda^2+\frac{1}{\lambda^2})^{-0.5}] \tag{15}$$

In equation (15), the length-diameter ratio of l/s expressed by $k_{l/s}$ is a material constant. For the exchange and correlation charge-density in the PA hydrogels, the length-diameter ratio ($k_{l/s}$) is determined by electrostatic repulsion and polarization. On the other hand, under a uniaxial tension, the mechanical loading will lead to the change of fractal geometry. The tensile and tearing loadings are able to change the values of $k_{l/s}$. Figure 6(a) shows that varying the values of $k_{l/s}$ leads to changes in the fractal shape from a globe to a double ellipsoid, resulting from the mechanical loading.

Effect of charge-density on the tearing force as a function of displacement has been further investigated using equation (15), and the corresponding parameters used in the calculation are listed in Table 3. Figure 6(b) shows the obtained calculation results for the tearing stress values as a function of displacement. The experimental data [45] of poly(NaSS-co-DMAEA-Q) PA hydrogels with various concentrations of $FeCl_3$ This are also included. Clearly, the simulation curves fit well with the experimental data [45]. Both the analytical and experimental results show that the tearing force of

poly(NaSS-co-DMAEA-Q) PA hydrogel is significantly increased from 0.35 N, 0.49 N, 0.60 N, 0.87 N to 1.05 N at the same displacement of λ=7.5 mm, with an increase in $FeCl_3$ concentration from 0 mol/L, 0.5 mol/L, 0.7 mol/L, 1 mol/L to 2 mol/L. Therefore, the effects of $FeCl_3$ concentration on the tearing forces of poly(NaSS-co-DMAEA-Q) PA hydrogel are similar to those of the tensile stress. The increased charge-density and changes in geometrical shapes of network structures are the two main reasons for the improvement of both the tensile and tearing mechanical strengths of the poly(NaSS-co-DMAEA-Q) PA hydrogels.

Table 3. Values of parameters used in equation (15) for tearing test of poly(NaSS-co-DMAEA-Q) PA hydrogel with various concentrations of Fe^{3+}.

$FeCl_3$ (mol/L)	$N_{el}k_BT$ (mN)	β	$\dfrac{fN^{3/2}b}{N_{el}L_{GC}}$	$k_{l/s}$
0	3.6			10.7
0.5	5.2			10.8
0.7	6.3	0.001	2	10.9
1	9.3			11.0
2	11.0			11.1

The divergences between the analytical and experimental results of the poly(NaSS-co-DMAEA-Q) PA hydrogels are calculated using the correlation index (R^2), and the obtained data are 87.34%, 92.88%, 90.33%, 86.27% and 94.98% for the concentrations of $FeCl_3$ increased from 0 mol/L, 0.5 mol/L, 0.7 mol/L, 1 mol/L to 2 mol/L, with the maximum error value $|\Delta\sigma|$<0.20 N, as shown in Figure 6(c).
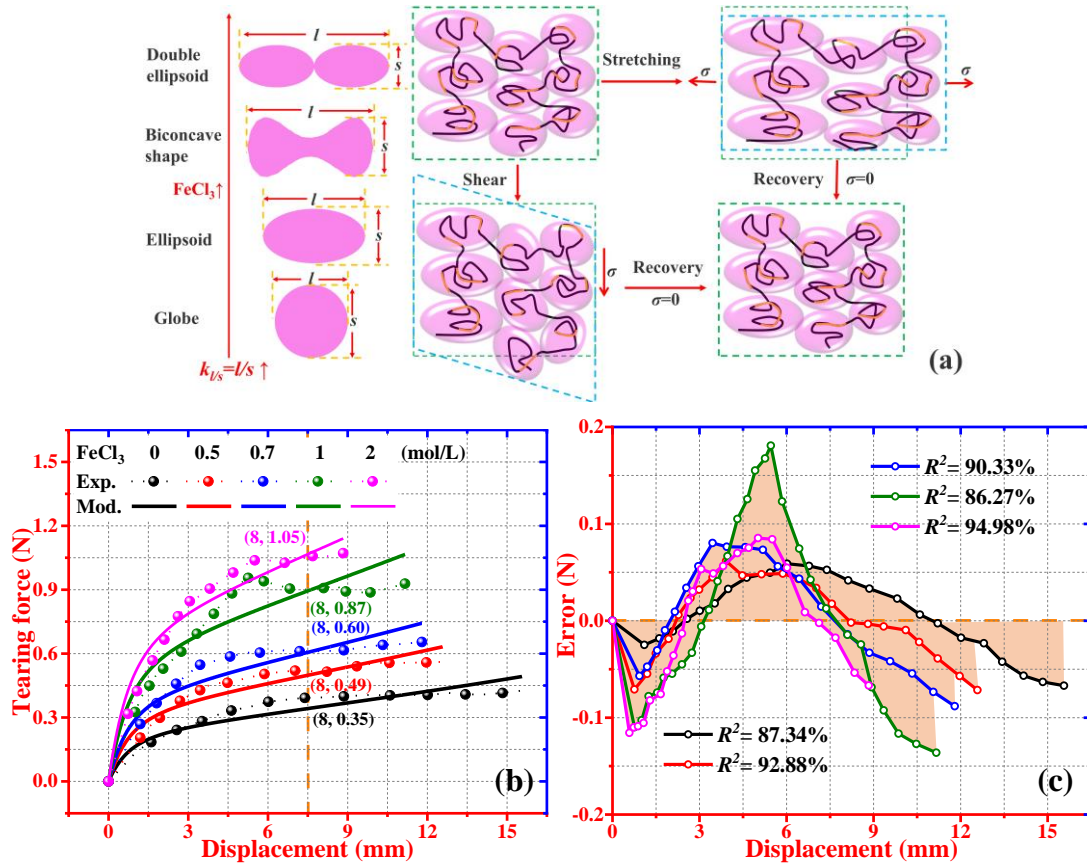
Figure 6. Comparisons of analytical and experimental results [45] for the tearing force as a function of displacement of poly(NaSS-co-DMAEA-Q) PA hydrogel. (a) Schematic illustrations of poly(NaSS-co-DMAEA-Q) PA hydrogel undergoing tensile and tearing loadings. (b) The tearing force-displacement curves, where concentrations of $FeCl_3$ are 0 mol/L, 0.5 mol/L, 0.7 mol/L, 1 mol/L and 2 mol/L. (c) Divergences of analytical and experimental results of stress.

To further verify the proposed model, effect of ionic strength on the mechanical behavior of the PA hydrogel has been investigated based on the equation (14). The obtained results of tensile stress as a function of elongation ratio are shown in Figure 7(a), which also includes the experimental data of poly(NaSS-co-DMAEA-Q) PA hydrogel reported in Ref. [45]. The parameters used in the equation (14) are listed in Table 4. Both the analytical and experimental results show that the stresses of poly(NaSS-co-DMAEA-Q) PA hydrogels are significantly increased from 0.36 MPa,

0.90 MPa to 1.87 MPa at the same elongation ratio of $\lambda=8$, with adding various ions of Na^+, Zn^{2+} and Fe^{3+}. Meanwhile, the divergences between the analytical and experimental results of the poly(NaSS-co-DMAEA-Q) PA hydrogels are calculated using the correlation index (R^2), which are 97.79%, 92.34% and 96.97% for NaCl, $ZnCl_2$ and $FeCl_3$, respectively, as shown in Figure 7(b).
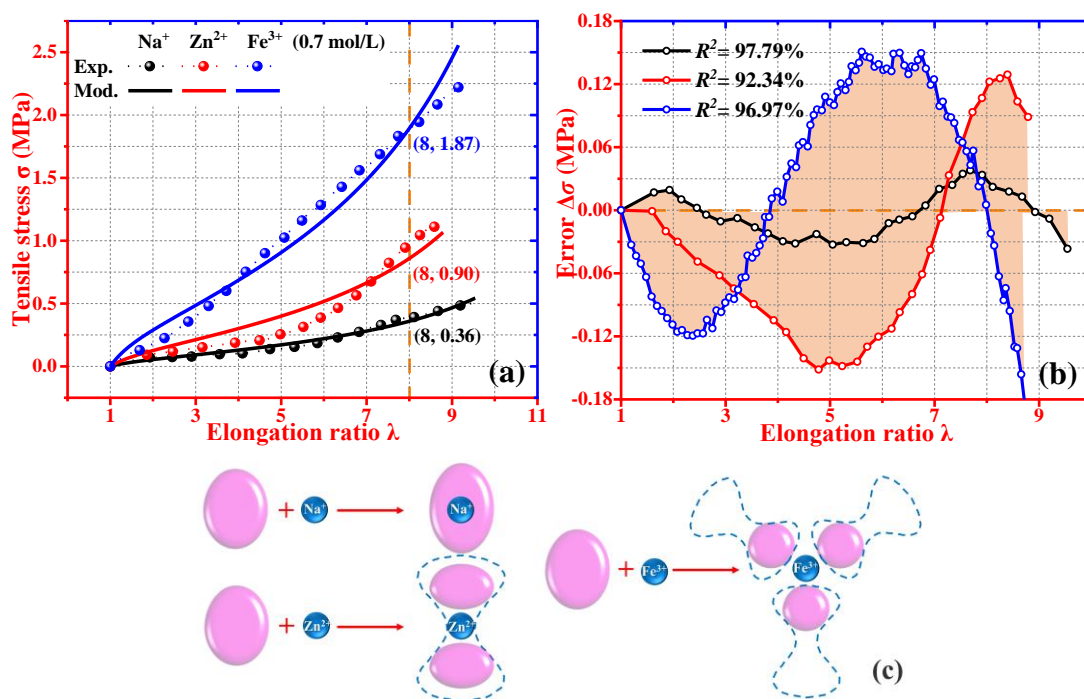

Figure 7. Effect of different ions (Na^+, Zn^{2+} and Fe^{3+}) on the constitutive stress-elongation ratio relationship in poly(NaSS-co-DMAEA-Q) PA hydrogel [45]. (a) The stress-elongation ratio curves. (b) Divergences of analytical and experimental results of stress. (c) Schematic illustrations of geometrical fractals of network structures in the poly(NaSS-co-DMAEA-Q) PA hydrogels with different ions of Na^+, Zn^{2+} and Fe^{3+}.

The working principles of different ions (Na^+, Zn^{2+} and Fe^{3+}) in the poly(NaSS-co-DMAEA-Q) PA hydrogel to improve the tensile stress are illustrated in Figure 7(c). Because of the different ionic strengths of Na^+, Zn^{2+} and Fe^{3+} ion doped hydrogels, it is able to achieve different geometrical shapes of the network structures,

e.g., ellipsoid fractal for Na^+, biconcave fractal for Zn^{2+} and triple ellipsoid fractal for Fe^{3+} [45]. Therefore, the mechanical behaviors of the poly(NaSS-co-DMAEA-Q) PA hydrogel after adding different ions are resulted from the various geometrical shapes of their network structures.

Table 4. Values of parameters used in equation (14) for poly(NaSS-co-DMAEA-Q) PA hydrogels doped with different ions of Na^+, Zn^{2+} and Fe^{3+}.

	$N_{el}k_BT$ (kPa)	β	$\dfrac{fN^{3/2}b}{N_{el}L_{GC}}$	$k_{l/s}$
Na^+	9.7			1.1
Zn^{2+}	22.5	0.012	0.1	1.2
Fe^{3+}	51.1			1.3

4. Discussion and conclusions

A self-consistent geometry fractal model has been proposed in this study to represent the mechanical behavior of the PA hydrogels. A complex fractal function is employed to characterize the geometrical shape of network structure, together with the consideration of charge-density, which is associated with the exchange and correlation charges generated in the hydrogel systems. The thermodynamics in the PA hydrogels undergoing exchange and correlation charge-density is formulated by the repulsive, polarization, conformational, elastic free energies. Then the self-consistent complex fractal function is used to analyze the geometrical shapes using the parameter of length-diameter ratio of l/s ($k_{l/s}$) with a repulsive free-energy function. This study is expected to provide a mathematical fractal to describe the polymer network and explore the mechanochemistry in PA hydrogel undergoing exchange and correlation charge-density of univalent and multivalent cations.

From a broader conceptual and practical perspective, this framework by designing and modifying the self-consistent geometrical fractals and shapes is well suitable for the achievement of the design of desired mechanical behaviors of the PA hydrogels. It can be applied for the hydrogel toughening using exchange and correlation charge-density, thus resolving the issues for difficult balance of deformability and toughness in the hydrogels. Moreover, the proposed model is also expected to guide the design strategy of PA hydrogels, with potential applications in actuators and soft robotics, which are driven by the exchange and correlation charge-density.

Finally, effectiveness of the proposed model has been verified using both FEA simulations and experimental results for the PA hydrogels. Comparisons between the analytical and experimental results reported from the literature [18,45] are presented, the toughening mechanism of PA hydrogel from mechanochemistry has been clarified, and the working principles of exchange and correlation charge-density of univalent and multivalent cations have been investigated and discussed. This study is expected to provide a fundamental framework to understand the mechanochemical constitutive relationship between charge-density and mechanics, as well as the toughening mechanisms in PA hydrogels.

References

[1] de Gennes P G 1992 Soft matter *Rev. Mod. Phys.* **64** 645−8

[2] Sun J Y, Zhao X, Illeperuma W R K, Chaudhuri O, Oh K H, Mooney D J, Vlassak J J and Suo Z 2012 Highly stretchable and tough hydrogels *Nature* **489** 133−6

[3] Daly A C, Riley L, Segura T and Burdick J A 2020 Hydrogel microparticles for biomedical applications *Nat. Rev. Mater.* **5** 20−43

[4] Matsuda T, Kawakami R, Namba R, Nakajima T and Gong J P 2019 Mechanoresponsive self-growing hydrogels inspired by muscle training *Science* **363** 504−8

[5] Yang C and Suo Z 2018 Hydrogel ionotronics *Nat. Rev. Mater.* **3** 125−42

[6] D'Agosto F, Rieger J and Lansalot M 2020 RAFT-mediated polymerization-induced self-assembly *Angew. Chem. Int. Ed.* **59** 8368−92

[7] Neto A M F and Salinas S R A 2005 *The Physics of Lyotropic Liquid Crystals Phase Transitions and Structural Properties* (New York: Oxford University Press)

[8] Kamata H, Akagi Y, Kayasuga-Kariya Y, Chung U and Sakai T 2014 "Nonswellable" hydrogel without mechanical hysteresis *Science* **343** 873−5

[9] Cui L, Zhang J, Zou J, Yang X, Guo H, Tian H, Zhang P, Wang Y, Zhang N, Zhuang X, Li Z, Ding J and Chen X 2020 Electroactive composite scaffold with locally expressed osteoinductive factor for synergistic bone repair upon electrical stimulation *Biomaterials* **230** 119617

[10] Long T, Li Y, Fang X and Sun J 2018 Salt-mediated polyampholyte hydrogels with high mechanical strength, excellent self-healing property, and satisfactory electrical conductivity *Adv. Funct. Mater.* **28** 1804416

[11] Huang Y, Li Z, Pei Z, Liu Z, Li H, Zhu M, Fan J, Dai Q, Zhang M, Dai L and Chunyi Zhi 2018 Solid-state rechargeable Zn//NiCo and Zn–Air batteries with ultralong lifetime and high capacity: The role of a sodium polyacrylate hydrogel electrolyte *Adv. Energy Mater.* **8** 1802288

[12] Zhang X, Yao D, Zhao W, Zhang R, Yu B, Ma G, Li Y, Hao D and Xu F J 2021 Engineering platelet-rich plasma based dual-network hydrogel as a bioactive wound dressing with potential clinical translational value *Adv. Funct. Mater.* **31** 2009258

[13] Zheng W J, An N, Yang J H, Zhou J X and Chen Y M 2015 Tough Al-alginate/poly(N-isopropylacrylamide) hydrogel with tunable LCST for soft robotics *ACS Appl. Mater. Inter.* **7** 1758−64

[14] Yang C, Liu Z, Chen C, Shi K, Zhang L, Ju X J, Wang W, Xie R and Chu L Y 2017 Reduced graphene oxide-containing smart hydrogels with excellent electro-response and mechanical properties for soft actuators *ACS Appl. Mater. Inter.* **9** 15758−67

[15] Zheng J, Jung S, Schmidt P W, Lodge T P and Reineke T M 2017 2-Hydroxyethylcellulose and amphiphilic block polymer conjugates form mechanically tunable and nonswellable hydrogels *ACS Macro Lett.* **6** 145−9.

[16] Gong J P, Katsuyama Y, Kurokawa T and Osada Y 2003 Double-network hydrogels with extremely high mechanical strength *Adv. Mater.* **15** 1155−8

[17] Yin H, King D R, Sun T L, Saruwatari Y, Nakajima T, Kurokawa T and Gong J P 2020 Polyzwitterions as a versatile building block of tough hydrogels: From polyelectrolyte complex gels to double-network gels. *ACS Appl. Mater. Inter.* **12** 50068−76

[18] Sun T L, Kurokawa T, Kuroda S, Ihsan A B, Akasaki T, Sato K, Haque M A, Nakajima T and Gong J P 2013 Physical hydrogels composed of polyampholytes demonstrate high toughness and viscoelasticity *Nat. Mater.* **12** 932−7

[19] Guo H, Sanson N, Hourdet D and Marcellan A 2016 Thermoresponsive toughening with crack bifurcation in phase-separated hydrogels under isochoric conditions *Adv. Mater.* **28** 58−64

[20] Lake G and Thomas A 1967 The strength of highly elastic materials *R. Soc. Lond. Proc. Ser. A Math. Phys. Eng. Sci.* **300** 108−19

[21] Anseth K S, Bowman C N and Brannon-Peppas L 1996 Mechanical properties of hydrogels and their experimental determination *Biomaterials* **17** 1647−57

[22] Naficy S, Brown H R, Razal J M, Spinks G M and Whitten P G 2011 Progress toward robust polymer hydrogels. *Aust. J. Chem.* **64** 1007−25

[23] Ahmed S, Nakajima T, Kurokawa K, Haque M A and Gong J P 2014 Brittle-ductile transition of double network hydrogels: Mechanical balance of two networks as the key factor *Polymer* **55** 914−23

[24] Luo F , Sun T L, Nakajima T , Kurokawa T , Zhao Y , Sato K, Ihsan A B , Li X, Guo H and Gong J P 2015 Oppositely charged polyelectrolytes form tough, self-healing, and rebuildable hydrogels *Adv. Mater.* **27** 2722–7

[25] Luo F , Sun T L, Nakajima T, Kurokawa T, Zhao Y, Ihsan A B, Guo H L, Li X F and Gong J P 2014 Crack blunting and advancing behaviors of tough and self-healing polyampholyte hydrogel *Macromolecules* **47** 6037−46

[26] Sun T L, Luo F, Hong W, Cui K, Huang Y, Zhang H J, King D R, Kurokawa T, Nakajima T and Gong J P 2017 Bulk energy dissipation mechanism for the fracture of tough and self-healing hydrogels *Macromolecules* **50** 2923−31

[27] Xiang Y H, Zhong D M, Wang P, Yin T H, Zhou H F, Yu H H, Baliga C, Qu S X and Yang W 2019 A physically based visco-hyperelastic constitutive model for soft materials *J. Mech. Phys. Solids* **128** 208−18

[28] Xing Z Y, Lu H B, Hossain M, Fu Y Q, Leng J S and Du S Y 2020 Cooperative dynamics of heuristic swelling and inhibitive micellization in double-network hydrogels by ionic dissociation of polyelectrolyte *Polymer* **186** 122039

[29] Xing Z Y, Lu H B, Sun A S, Fu Y Q, Shahzad M W and Xu B B 2021 Understanding complex dynamics of interfacial reconstruction in polyampholyte hydrogels undergoing mechano-chemo-electrotaxis coupling. *J. Phys. D: Appl. Phys.* **54** 085301

[30] Hofzumahaus C, Strauch C and Schneider S 2021 Monte Carlo simulations of weak polyampholyte microgels: pH-dependence of conformation and ionization *Soft Matter* **17** 6029−43

[31] Cui K, Sun T L, Kurokawa T, Nakajima T, Nonoyama T, Chen L and Gong J P 2016 Stretching-induced ion complexation in physical polyampholyte hydrogels *Soft Matter* **12** 8833−40

[32] Venkata S P, Cui K, Guo J, Zehnder A T, Gong J P and Hui C-Y 2021 Constitutive modeling of strain-dependent bond breaking and healing kinetics of chemical polyampholyte (PA) gel *Soft Matter* **17** 4161−9

[33] Dobrynin A V, Obukhov S P and Rubinstein M 1999 Long-range multichain adsorption of polyampholytes on a charged surface *Macromolecules* **32** 5689−700

[34] Dobrynin A V, Zhulina E B and Rubinstein M 2001 Structure of adsorbed polyampholyte layers at charged objects *Macromolecules* **34** 627−39

[35] Dobrynin A V, Colby R H and Rubinstein M 2004 Polyampholytes *J. Poly. Sci. Pol. Phys.* **42** 3513−38

[36] Shin J, Cherstvy A G and Metzler R 2014 Sensing viruses by mechanical tension of DNA in responsive hydrogels *Phys. Rev. X* **4** 021002

[37] Caetano D L Z, de Carvalho S J, Metzler R and Cherstvy A G 2017 Critical adsorption of periodic and random polyampholytes onto charged surfaces *Phys. Chem. Chem. Phys.* **19** 23397−413

[38] Zhu Q and Bi X 2022 Dynamics of erythrocytes in oscillatory shear flows: effects of S/V ratio *Soft Matter* **18** 964−74

[39] Treloar L R G 1975 *The Physics of Rubber Elasticity* (New York: Oxford University press)

[40] Dobrynin A V and Carrillo J M Y 2011 Universality in nonlinear elasticity of biological and polymeric networks and gels *Macromolecules* **44** 140−6

[41] Carrillo J M Y, MacKintosh F C and Dobrynin A V 2013 Nonlinear elasticity: from single chain to networks and gels *Macromolecules* **46** 3679−92

[42] Xing Z Y, Li Z H, Lu H B and Fu Y Q 2021 Self-assembled topological transition via intra- and inter-chain coupled binding in physical hydrogel towards mechanical toughening *Polymer* **235** 124268

[43] Xing Z Y, Shu D W, Lu H B and Fu Y Q 2022 Untangling the mechanics of entanglements in slide-ring gels towards both super-deformability and toughness *Soft Matter* **18** 1302−9

[44] Ji B and Gao H 2004 Mechanical properties of nanostructure of biological materials *J. Mech. Phys. Solids* **52** 1963−90

[45] Huang Y, Xiao L, Zhou J, Liu T, Yan Y, Long S and Li X 2021 Strong tough polyampholyte hydrogels via the synergistic effect of ionic and metal–ligand Bonds *Adv. Funct. Mater.* **31** 2103917